Energy & Environmental Science

Accepted Manuscript

This article can be cited before page numbers have been issued, to do this please use: X. Cui, Y. Chen, M. Zhang, Y. Harn, J. Qi, L. Gao, Z. L. Wang, J. Huang, Y. Yang and Z. Lin, *Energy Environ. Sci.*, 2020, DOI: 10.1039/C9EE03937F.

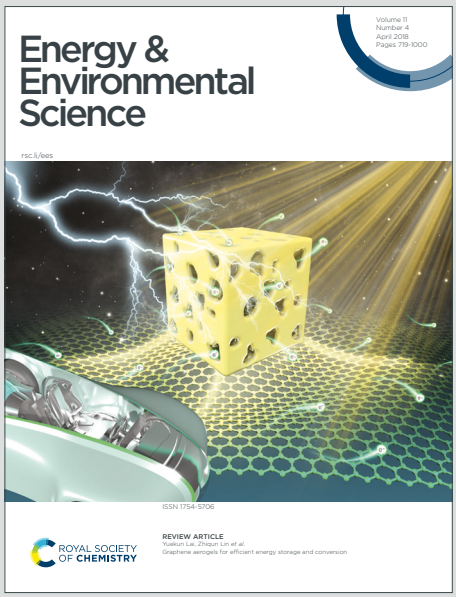

ROYAL SOCIETY OF CHEMISTRY

rsc.li/ees

View Article Online
DOI: 10.1039/C9EE03937F

ARTICLE

Tailoring Carrier Dynamics in Perovskite Solar Cells via Precise Dimension and Architecture Control and Interfacial Positioning of Plasmonic Nanoparticles

Received 00th January 20xx,
Accepted 00th January 20xx

DOI: 10.1039/x0xx00000x

Xun Cui,[ab#] Yihuang Chen,[a#] Meng Zhang,[a] Yeu Wei Harn,[a] Jiabin Qi,[a] Likun Gao,[a] Zhong Lin Wang,[a] Jinsong Huang,[c] Yingkui Yang,*[b] and Zhiqun Lin*[a]

Placing plasmonic nanoparticles (NPs) in close proximity to semiconductor nanostructures renders effective tuning of the optoelectronic properties of semiconductors through the localized surface plasmon resonance (LSPR)-induced enhancement of light absorption and/or promotion of carrier transport. Herein, we report on, for the first time, the scrutiny of carrier dynamics of perovskite solar cells (PSCs) via sandwiching monodisperse plasmonic/dielectric core/shell NPs with systematically varied dielectric shell thickness yet fixed plasmonic core diameter within electron transport layer (ETL). Specifically, a set of Au NPs with precisely controlled dimensions (i.e., fixed Au core diameter and tunable SiO_2 shell thickness) and architectures (plain Au NPs and plasmonic/dielectric Au/SiO_2 core/shell NPs) are first crafted by capitalizing on the star-like block copolymer nanoreactor strategy. Subsequently, these monodisperse NPs are sandwiched between the two consecutive TiO_2 ETLs. Intriguingly, there exists a critical dielectric SiO_2 shell thickness, below which hot electrons from Au core are readily injected to TiO_2 (i.e., hot electron transfer (HET)); this promotes local electron mobility in TiO_2 ETL, leading to improved charge transport and increased short-circuit current density (J_{sc}). It is also notable that the HET effect moves up the Fermi level of TiO_2, resulting in an enhanced built-in potential and open-circuit voltage (V_{oc}). Taken together, the PSCs constructed by employing a sandwich-like TiO_2/Au NPs/TiO_2 ETL exhibit both greatly enhanced J_{sc} and V_{oc}, delivering champion PCEs of 18.81% and 19.42% in planar and mesostructured PSCs, respectively. As such, the judicious positioning of rationally designed monodisperse plasmonic NPs in ETL affords effective tailoring of carrier dynamics, thereby providing a unique platform for developing high-performance PSCs.

Broder context

Plasmonic nanoparticles (NPs) have been introduced in photovoltaic devices, aiming initially at increasing light absorption. In the case of perovskite solar cells (PSCs) incorporating with plasmonic NPs, recent reports have shown the improvement of the photovoltaic performance; however, negligible light absorption enhancement was observed. In this context, investigaton into the mechanisms of plasmonic enhancement in PSCs is valuable and urgently needed. In addition, the dielectric SiO_2 shell thickness can significantly affect the electronic characteristics of Au/SiO_2 core/shell NPs. Clearly, the ability to systematically alter the SiO_2 shell thickness at the nanometer scale enables a tunable electronic characteristic of Au/SiO_2 core/shell NPs. However, while highly desirable, it is challenging to precisely and systematically control the dimension and architecture of Au/SiO_2 core/shell NPs at nanoscale. In this work, we develop a robust amphiphilic star-like block copolymer nanoreactor strategy to create a set of monodisperse plasmonic NPs of different sizes and architectures (i.e., plain Au and Au/SiO_2 core/shell NPs), and subsequently scrutinize, for the first time, the effects of the dielectric SiO_2 shell thickness and the positioning of plasmonic NPs on the charge carrier dynamics and thus the performance of PSCs. This study offers insight into the tailoring of charge carrier dynamics in PSCs via rational design and placement of monodisperse plasmonic/dielectric NPs with tunable dielectric shell thickness to achieve high-performance PSCs.

Introduction

Recent research has witnessed unprecedented advances in organolead halide perovskite solar cells (PSCs) with power conversion efficiency (PCE) leaping from approximately 3% to 25.2% comparable to that of silicon-based solar cells.[1-6] Various effective strategies have been developed for raising the performance of PSCs, including perovskite absorber design and crystal growth,[7-10] defect passivation,[11] and interface engineering[12, 13]. Among them, interface engineering stands out as an effective means of enabling control over carrier dynamics within the entire device. The implementation of plasmonic nanoparticles (NPs) in either the absorber or carrier transport layers of a solar cell represents a promising route to bettering the harvesting of incident light[14] via localized surface plasmon resonance (LSPR) effect[15-17] and engineering the carrier dynamics (i.e., promoting carrier transport and collection)[18-20] via regulating their optical and electronic characteristics. In the

[a] School of Materials Science and Engineering, Georgia Institute of Technology, Atlanta, GA 30332, USA. E-mail: zhiqun.lin@mse.gatech.edu
[b] Key Laboratory of Catalysis and Energy Materials Chemistry of Ministry of Education & Hubei Key Laboratory of Catalysis and Materials Science, South-Central University for Nationalities, Wuhan 430074, China. E-mail: ykyang@mail.scuec.edu.cn
[c] Department of Applied Physical Sciences, University of North Carolina, Chapel Hill, NC 27599, USA.
[d] # equal contribution.

† Electronic Supplementary Information (ESI) available: Detailed description of the experimental methods and additional data and figures. See DOI: 10.1039/x0xx000x

particular case of PSCs incorporating with plasmonic NPs, recent reports have indeed shown the improvements of the photovoltaic performance.[18-20] However, negligible light absorption enhancement was observed. In this context, performing fundamental research to gain deep insights into the plasmonic enhancement mechanisms is valuable and urgently needed. Notably, for the most commonly used TiO_2 electron transport layer (ETL) in PSCs, its trap states need to be filled up by photo-generated electrons under illumination to render TiO_2 with an improved photoconductivity.[21] Placing Au NPs in close contact with TiO_2 imparts the hot electron transfer (HET) from Au NPs to occupy the trap states of TiO_2, leading to increased charge carrier density in TiO_2. Consequently, the charge mobility of TiO_2 increases that facilitates the extraction of photo-generated electrons from absorber at the TiO_2/absorber interface and their transport.

The strength of LSPR effect of noble metal NPs (e.g., Au and Ag) depends heavily on the NP size. For hot electrons, they are efficiently generated in noble metal nanostructures with a size less than 20 nm.[22] Another factor largely affecting the strength of LSPR effect is the dielectric property of the surrounding medium. It has been reported that the dielectric SiO_2 shell of Au/SiO_2 core/shell NP prohibits HET generated from Au from jumping over the Schottky barrier unless the SiO_2 thickness is less than its tunneling barrier height (~3 nm).[23] Clearly, the ability to systematically alter the SiO_2 shell thickness at the nanometer scale enables a tunable electronic characteristic of Au/SiO_2 core/shell NPs. This, however, has yet to be largely explored. In this context, despite recent advances in implementing the LSPR effect of plasmonic NPs in PSCs, our understanding on how the dielectric shell of varied thickness influences the HET of the plasmonic core and in turn the performance of the resulting PSCs remains comparatively elusive.

Until now, it is still highly desirable but challenging yet to precisely and systematically control the dimension and architecture of plasmonic NPs at the nanoscale. Herein, we develop a robust amphiphilic-star-like-block-copolymer nanoreactor strategy to create an array of monodisperse plasmonic NPs of different sizes and architectures (i.e., plain Au and Au/SiO_2 core/shell NPs), and subsequently scrutinize, for the first time, the effects of dielectric SiO_2 shell thickness and the positioning of plasmonic NPs (i.e., sandwiched within TiO_2 ETL (scenario 1) and at the perovskite/TiO_2 ETL interface (scenario 2)) on the charge carrier dynamics and thus the performance of PSCs. First, two amphiphilic star-like block copolymers, namely, poly(acrylic acid)-*block*-polystyrene (denoted PAA-*b*-PS) and poly(4-vinyl pyridine)-*block*-poly(*t*-butyl acrylate)-*block*-poly(ethylene oxide) (denoted P4VP-*b*-P*t*BA-*b*-PEO), with well-defined molecular weight and low polydispersity index are synthesized via controlled living radical polymerization. They were then exploited as nanoreators to craft uniform Au NPs and Au/SiO_2 core/shell NPs, respectively. It is important to note that Au and SiO_2 are template-grown by capitalizing on P4VP and PAA (hydrolyzed from P*t*BA) blocks, respectively. Thus, the Au core diameter and the SiO_2 shell thickness can be precisely controlled by tuning the molecular weight of the inner P4VP and intermediate P*t*BA blocks via controlling atom transfer radical polymerization (ATRP) time of 4-vinyl pyridine (4VP) and *t*-butyl acrylate (*t*BA), respectively. As a result, a set of Au/SiO_2 NPs at the constant Au core diameter and different SiO_2 shell thickness are conveniently produced.

Undoubtedly, this effective and robust strategy ensures the subsequent scrutinize of the effects of dielectric SiO_2 shell thickness and the mechanism research. By incorporating plain Au NPs and Au/SiO_2 NPs of varied SiO_2 shell thickness (t_{SiO2} = 2, 6 and 10 nm at fixed D_{Au} = 12 nm) in PSCs with two different positioning scenarios, that is, encapsulated inside the TiO_2 ETL and deposited at the perovskite/TiO_2 ETL interface, we uncover the mechanism with which the charge carrier dynamics of PSCs is affected. Intriguingly, rather than the optical effect of plasmonic NPs, their electronic characteristic was found to markedly improve photovoltaic performance of PSCs, as substantiated by time-resolved photoluminescence spectroscopy (TRPL), intensity modulated photocurrent spectroscopy (IMPS), and intensity modulated photovoltage spectroscopy (IMVS) measurements. Investigation into the effect of the SiO_2 shell thickness reveals the existence of a critical dielectric SiO_2 shell thickness, below which HET from Au core to TiO_2 ETL readily occurs, thereby improving electron mobility in TiO_2 ETL due to the filled trap states in TiO_2 and resulting in improved charge transfer from perovskite to TiO_2 and transport within TiO_2 and thus increased short-circuit current density (J_{sc}). Concurrently, the carrier density in TiO_2 is improved due to the HET effect that moves up the Fermi level of TiO_2 and reduces its work function, giving rise to an enhanced open-circuit voltage (V_{oc}) as evidenced by Kelvin probe measurement and Mott-Schottky analysis. In sharp contrast, beyond the critical SiO_2 shell thickness (i.e., 6 nm and 10 nm), only slight increase of J_{sc} was observed due to the LSPR-induced charge separation/transfer as a result of near electromagnetic field (NEF) enhancement effect within the TiO_2 ETL. The J_{sc} is yet much smaller than the device with the SiO_2 shell below the critical thickness. Moreover, owing to the absence of HET, no V_{oc} enhancement for plasmonic NPs with 6-nm and 10-nm SiO_2 shell-incorporated devices was seen.

The optimized planar and mesostructured PSCs based on $FA_{0.85}MA_{0.15}PbI_{2.55}Br_{0.45}$ absorber assembled with a sandwich-shaped ETL (i.e., impregnating Au NPs within TiO_2 ETL) deliver champion PCEs of 18.81% and 19.42%, respectively. It is notable that the devices with the sandwiched placement of plasmonic NPs within ETL (scenario 1) outperform those of constructed by situating plasmonic NPs at the perovskite/TiO_2 interface (scenario 2). This is not surprising as plamonic NPs largely function as the recombination center for charge carriers, leading to decreased J_{sc} and V_{oc} and thus lowered PCEs. This study offers insight into the tailoring of charge carrier dynamics at interface of PSCs via rational design and placement of monodisperse plasmonic/dielectric NPs of tunable dielectric shell thickness to achieve plasmonic enhancement-enabled high-performance PSCs.

DOI: 10.1039/C9EE03677F

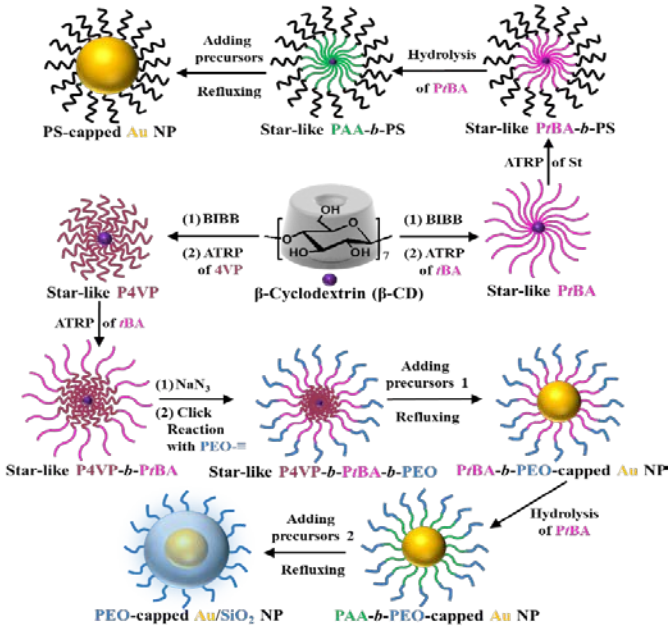

Figure 1. Stepwise representation of synthetic route to plain Au and Au/SiO_2 core/shell NP by capitalizing on amphiphilic star-like poly(acrylic acid)-*block*-polystyrene (PAA-*b*-PS) diblock copolymer and poly(4-vinyl pyridine)-*block*-poly(*t*-butyl acrylate)-*block*-poly(ethylene oxide) (P4VP-*b*-P*t*BA-*b*-PEO) triblock copolymer, respectively, as nanoreactors.

Results and discussion

Synthesis and characterization of plain Au and Au/SiO_2 core/shell nanoparticles.

Due to the branched yet compact architecture, amphiphilic star-like block copolymer with each block copolymer arm covalently connected to a central small molecular core form a unimolecular micelle in solution. Such unimolecular micellar architecture is static rather than dynamic as in conventional micelle produced from self-assembly of linear amphiphilic block copolymers in selective solvent. The conventional micelle may be readily disassembled upon the change of experimental conditions (e.g., concentration, solvent, pH, temperature, etc.). Nonetheless, the structurally stable unimolecular micelle of amphiphilic star-like block copolymer is then employed as nanoreactor for crafting inorganic NPs. **Figure 1** depicts the synthetic routes to plain Au NP and Au/SiO_2 core/shell NP using the amphiphilic star-like PAA-*b*-PS diblock copolymers (central panel; first row) and P4VP-*b*-P*t*BA-*b*-PEO triblock copolymers (central panel; third row), respectively, as nanoreactors. Amphiphilic PAA-*b*-PS is synthesized via a sequential atom transfer radical polymerization (ATRP) of *t*-butyl acrylate (*t*BA) and styrene (St) from a *β*-cyclodextrin-based macroinitiator, followed by the hydrolysis of inner poly(*t*-butyl acrylate) (P*t*BA) blocks (**Table S1**).[24, 25] The coordination interaction between the carboxyl groups (-COOH) of PAA blocks and the metal moiety of Au precursors ($HAuCl_4$) preferentially partitions the precursors within the regime occupied by inner hydrophilic PAA blocks of star-like PAA-*b*-PS diblock copolymer, leading to the formation of Au NPs intimately capped by outer PS blocks (i.e., PS-capped Au NPs; left panel, first row). Similarly, amphiphilic P4VP-*b*-P*t*BA-*b*-PEO is prepared via a combination of sequential ATRP of 4-vinyl pyridine (4VP) and *t*BA from a *β*-cyclodextrin-based macroinitiator with a click reaction (**Table S1**).[25, 26] Likewise, the inner hydrophilic P4VP blocks and intermediate hydrophilic poly(acrylic acid) (PAA) blocks converted from the hydrolysis of hydrophobic P*t*BA render the formation of Au core (from central to right panels; third row; **Figure 1**) and SiO_2 shell (from right to left panels; fourth row; **Figure 1**) through the strong coordination interactions between the precursors ($HAuCl_4$ for Au and tetraethoxysilane (TEOS) for SiO_2) and the functional groups in P4VP (pyridal groups) and PAA (-COOH groups) blocks, respectively. It is noteworthy that the Au core diameter and the SiO_2 shell thickness in PEO-capped Au/SiO_2 core/shell NP can be precisely controlled by tailoring the molecular weights (i.e., lengths) of the inner P4VP and intermediate P*t*BA blocks, respectively, via controlling the sequential ATRP time of 4VP and *t*BA due to the living radical polymerization characteristic of ATRP.[27]

As discussed above, hot electrons are effectively generated when the size of plasmonic nanostructures less than 20 nm.[22] Thus, in order to explore the shell thickness-dependent plasmonic effect of Au NPs and Au/SiO_2 NPs introduced in PSCs, the Au core diameter needs to be less than 20 nm and remains constant for comparison. **Figure 2** compares the TEM images of as-synthesized plain PS-capped Au NPs (D_{Au} = 12 nm; **Figure 2a**) and PEO-capped Au/SiO_2 core/shell NPs at a constant D_{Au} of 12 nm and judiciously varied SiO_2 shell thickness of 2, 6 and 10 nm (**Figure 2b-d**). All NPs are highly uniform with narrow size distribution (**Table S2**). Clearly, the nanoreactor strategy provides remarkable flexibility in synthesizing core/shell NPs with tailored shell thickness via controlling the molecular

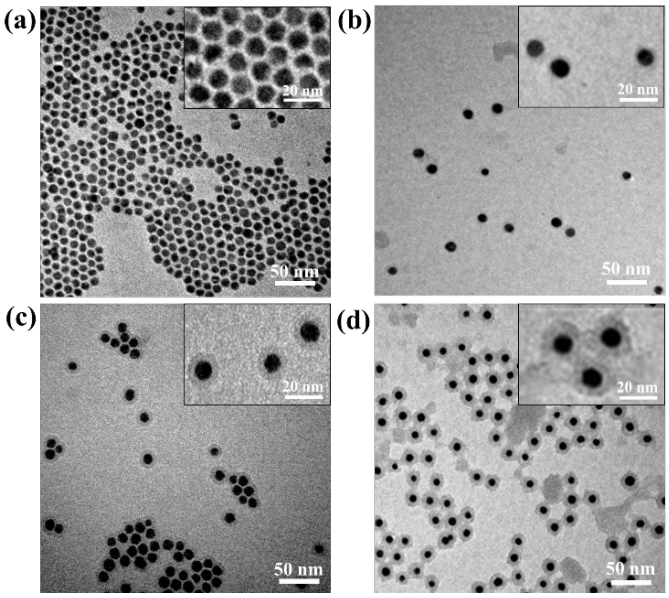

Figure 2. TEM images of plain Au and Au/SiO_2 core/shell NPs at a fixed Au core diameter and varied SiO_2 shell thickness. (a) Plain Au NPs with a diameter of 12 nm. (b-d) Au/SiO_2 core/shell NPs. The diameter of the Au core and thickness of the SiO_2 shell are as follows: (b) 12 nm Au and 2 nm SiO_2, (c) 12 nm Au and 6 nm SiO_2, and (d) 12 nm Au and 10 nm SiO_2, respectively. Insets show the close-ups of NPs.

weight of the P*t*BA block solely during ATRP of *t*BA (**Figure 2b-d**). The Au core appears darker and is surrounded by the lighter SiO_2 shell, as clearly evidenced by TEM imaging.

Impacts of interfacial positioning and dielectric SiO_2 shell thickness on device performance.

The plain Au NPs and Au/SiO_2 core/shell NPs are then exploited to scrutinize the effects of dielectric SiO_2 shell thickness and the positioning of these plasmonic NPs on charge carrier dynamics in PSCs and the resulting device performance. First, we optimized the thickness of TiO_2 ETL (see **Figure S1**, **Figure S2a-d**, **Table S3**, and **Note S1** for detailed optimization process) and found that a double-layered TiO_2 film as ETL favors an optimum device performance. We note that all polymer ligands (PS as in PS-capped Au NPs, and PEO as in PEO-capped Au/SiO_2 core/shell NPs) are removed during the sintering treatment of TiO_2 ETL. Appropriate positioning of plasmonic NPs can effectively improve the photovoltaic performance of PSCs. In our study, two different assembly scenarios for incorporating plasmonic NPs into PSCs are invoked, that is, either sandwiched within TiO_2 ETL (scenario 1, **Figure 3a**) or incorporated at the perovskite $CH_3NH_3PbI_3$/TiO_2 ETL interface (scenario 2, **Figure S3**).

As the first attempt, the plasmonic NPs (i.e., plain Au NPs and Au/SiO_2 core/shell NPs) are deposited at the $CH_3NH_3PbI_3$/TiO_2 interface (scenario 2) via spin-coating. It was found that the direct contact between Au NPs and perovskite $CH_3NH_3PbI_3$ absorber deteriorates the device performance as the Au NPs acts as the recombination center for photo-generated charge carriers in perovskite film as reported in literature.[20] In scenario 2, devices fabricated with either plain Au NPs or Au/SiO_2 core/shell NPs with a very thin SiO_2 shell of 2 nm placed at the $CH_3NH_3PbI_3$/TiO_2 interface yield poorer performance than that of control device (**Figure S4** and **Table S4**). For Au/SiO_2 core/shell NPs with relatively thicker shells (6 nm and 10 nm) placed at the $CH_3NH_3PbI_3$/TiO_2 interface, slightly improved device performances were observed although the relatively thicker SiO_2 shells could minimize carrier recombination on the Au core (**Figure S4** and **Table S4**). Such performance improvement can be credited to the LSPR-induced enhancement of light absorption and promotion of carrier transport and collection.[28]

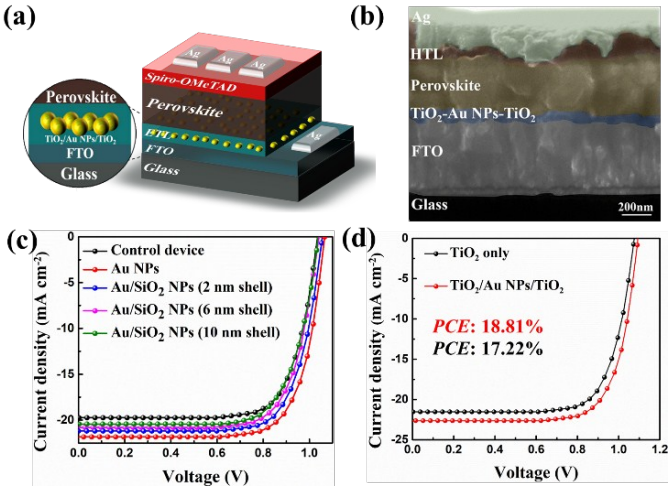

Figure 3. (a) Schematic of planar PSC (denoted p-PSC) assembled by capitalizing on plain Au NPs sandwiched between a double-layer TiO_2 ETL. (b) Cross sectional SEM image of p-PSC fabricated on a sandwiched TiO_2 ETL (i.e., scenario 1: TiO_2/Au NPs/TiO_2 ETL). (c) *J-V* characteristics of perovskite $CH_3NH_3PbI_3$ solar cells constructed with TiO_2 only (control device) and with Au NPs and Au/SiO_2 NPs sandwiched between a double-layer TiO_2 as ETLs. (d) *J-V* characteristics of perovskite $FA_{0.85}MA_{0.15}PbI_{2.55}Br_{0.45}$ solar cells with (PCE = 18.81%) and without Au NPs (PCE = 17.22%) sandwiched between a double-layer TiO_2 ETL.

We now turn our attention to investigate the dielectric SiO_2 shell thickness-dependent charge carrier dynamics in PSC where plasmonic NPs are sandwiched within TiO_2 ETL (scenario 1; **Figure 3a**). Unless otherwise specified, the PSCs discussed below are assembled using $CH_3NH_3PbI_3$ as the absorber in a planar device configuration (denoted p-PSCs). In contrast to scenario 2, a direct contact between plasmonic Au and perovskite absorber is effectively prevented in scenario 1. As a result, the detrimental recombination pathway can be prohibited, and accordingly the charge carrier extraction efficiency in PSC is improved. **Figure 3a** depicts the device configuration of a planar PSC. A cross-sectional scanning electron microscopy (SEM) image is shown in **Figure 3b**. **Figure 3c** compares representative current density-voltage (*J-V*) curves of devices constructed using a pristine TiO_2 ETL (control device) and a double-layer TiO_2 ETL sandwiched with Au NPs and Au/SiO_2 core/shell NPs of different SiO_2 shell thickness. The detailed statistics of parameters is summarized in **Table S5**. It was found that all devices based on plain Au NPs and Au/SiO_2 core/shell NPs with varied SiO_2 shell thickness show improved performance. A scrutiny of the *J-V* curves and parameters statistics reveals a shell-dependent device performance. First, for devices based on Au/SiO_2 NPs with relatively thicker SiO_2 shell (6 nm and 10 nm), the enhanced PCE is primarily determined by the J_{sc}, whereas the V_{oc} and fill factor (*FF*) remain nearly constant. In sharp contrast, for devices constructed using plain Au NPs and Au/SiO_2 NPs with a very thin SiO_2 shell (2 nm), both J_{sc} and V_{oc} are markedly increased when compared to control device (i.e., in the absence of incorporation of plasmonic NPs within the TiO_2 ETL). Such an observation suggests the notably different underlying mechanisms responsible for the performance enhancement of PSCs for these devices. The V_{oc} improvement induced by the introduction of plain Au NPs and Au/SiO_2 NPs of a 2 nm SiO_2 shell thickness is likely associated with the HET effect that may change the surface potential of the TiO_2 ETL, thus decreasing energy barrier for carrier transport from perovskite photoactive layer to TiO_2 ETL and increasing the built-in potential.[19, 29] The increased V_{oc} was not observed for the Au core capped with a relatively thicker SiO_2 shell (6 nm and 10 nm). For Au/SiO_2 core/shell NPs, the hot electrons that reach the Au/SiO_2 interface can effective overcome the electron tunneling barrier of the insulating SiO_2 at the SiO_2 thickness of $\leqslant$ 3 nm according to the literature.[23] Thus, for 6 nm and 10 nm SiO_2 shell in present study, it is highly unlikely that the hot electrons from Au core could transfer to the conduction band (CB) of TiO_2, suggesting that the HET effect does not play a role in this particular case. In addition, relatively thicker SiO_2 shells exhibit a suppression in the enhancement of J_{sc} due primarily to

View Article Online
DOI: 10.1039/C9EE03937F

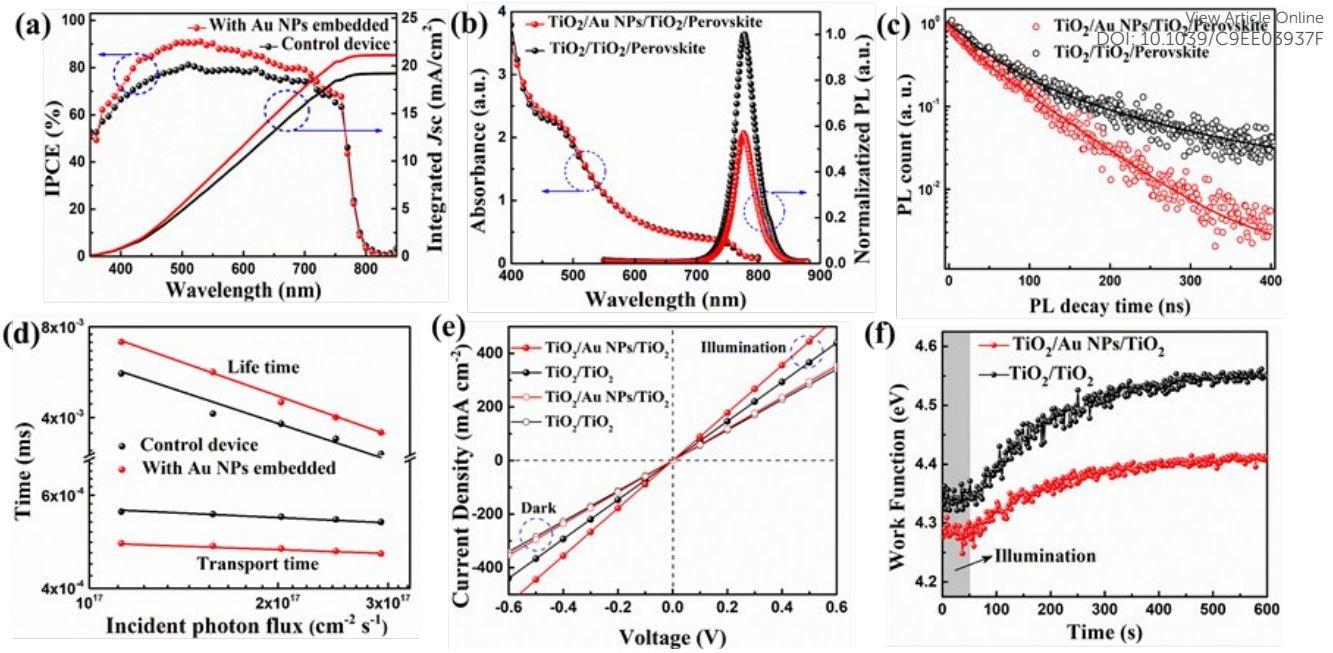

Figure 4. (a) IPCE spectra, (b) UV-vis absorption and time-integrated PL spectra, (c) time-resolved PL spectra, (d) charge transit time and carrier lifetime, (e) *J-V* curves of conductivity test under illumination and dark conditions, and (f) work function changes after illumination measured by the Kelvin probe force microscope.

the restrained interaction between the localized electromagnetic field originated from Au and the carriers. Therefore, a thinner insulating SiO_2 shell of <3 nm is highly desirable for not only enabling a strong coupling of Au/SiO_2 NPs with the surrounding TiO_2 NPs, but also allowing hot carrier transfer over the SiO_2 tunneling barrier. As a result, devices based on both plain Au NPs and Au/SiO_2 NPs with a 2 nm thick SiO_2 yield better performance, especially for the plain Au NPs-based device, achieving an optimal average PCE of 17.30% (**Table S5**). **Figure S5** show the statistical results of device characteristics by varying the loading level of Au NPs sandwiched between a double-layer TiO_2 ETL in the p-PSCs. The optimal concentration of Au NPs toluene solution was found to be 3 mg ml^{-1}. At this concentration, both the average J_{sc} and V_{oc} of Au NPs-based PSCs were improved, resulting in an absolute improvement of PCE. It is also important to note that there is no significant discrepancy between the reverse and forward device parameters (**Figure S6**), indicating less hysteresis and higher reliability of the *J-V* characteristics. Steady-state output PCE and photocurrent density of control device and the device based on Au NPs sandwiched between a double-layer TiO_2 are shown in **Figure S7**. Clearly, the Au NPs-incorporated device delivers a stable output J_{sc} of 20.2 mA cm^{-2} and a PCE of 16.5 %. While for the control device, the output J_{sc} and PCE are reduced to 18.30 mA cm^{-2} and 14.3%, respectively, indicating that the introduction of plain Au NPs in TiO_2 ETL renders a stable device with a higher output energy under the standard sunlight. **Figure S8** summarize the statistic distributions of J_{sc}, V_{oc}, *FF* and PCE of control device and Au NPs-incorporated device. The average trend of the parameters is consistent with that of the representative devices shown in **Figure 3c** (i.e., control device and Au NPs-incorporated device) and **Table S5**. It is clear that the most probable J_{sc} of 21.5 mA cm^{-2} and V_{oc} of 1.06 V are achieved from the Au NPs-incorporated device, which are higher than those of control device (J_{sc} = 20.0 mA cm^{-2} and V_{oc} = 1.03 V). Notably, by further optimizing the perovskite layer using a mixed $FA_{0.85}MA_{0.15}PbI_{2.55}Br_{0.45}$, the PCE of the resulting device that incorporates sandwiched Au NPs within TiO_2 ETL is further improved from 17.22% (control device without Au NPs introduced into TiO_2 ETL) to 18.81% (**Figure 3d**). The judicious sandwiching of Au NPs between a double-layer TiO_2 effectively circumvents the direct contact between Au NPs and the perovskite absorber, representing a critical step toward achieving high-performance devices. It is noteworthy that the assembly scenario 1 (**Table S5**) yields higher device efficiencies over those from the assembly scenario 2 (**Table S4**).

Scrutiny of mechanisms and charge carrier dynamics.

In order to explore the mechanism that underpins the performance enhancement of PSCs based on Au NPs-incorporated TiO_2 ETL, incident photo-to-electron conversion efficiency (IPCE) measurement was first performed to evaluate the increased J_{sc} of device (**Figure 4a**). It is clear that the IPCE is improved via the introduction Au NPs, yet the enhancement is broadly distributed over the entire spectral range and does not specifically follow the plasmonic absorption of Au NPs. It is noteworthy that both the maximal IPCE (**Figure 4a**) and IPCE enhancement (**Figure S9**) were found to be around 525 nm, matching with the absorption peak of Au NPs and thus likely provides some evidence that the NEF enhancement of Au NPs indeed induces a PCE improvement of PSCs. The UV-vis absorption spectra of the perovskite layer deposited on the TiO_2 ETL with and without incorporation of Au NPs are shown in **Figure 4b**. A very marginal improvement was seen for the Au NPs-incorporated sample in the range of specific absorption wavelengths associated with Au NPs. We also found that there

View Article Online
DOI: 10.1039/C9EE03937F

is no obvious morphology difference between perovskite films deposited on the double-layer TiO_2 ETL with and without the embedding of Au NPs (**Figure S2d,e**). The domain size and surface coverage are similar in the two films with high uniformity, which ensure a good light harvesting capability. Taken together, the incorporation of as-prepared Au NPs in PSCs exerts a minor influence on the absorption and morphology. The simulation results show that the LSPR effect leads to a substantially non-uniform electric field distribution, which depends heavily on the wavelength of the incident light (**Figure S10**). However, this wavelength-dependent difference was not obviously observed in the UV-vis absorption measurement (**Figure 4b**). This may be attributed to the large light absorption coefficient of perovskite as well as the low loading of Au NPs, suggesting that the J_{sc} enhancement cannot be attributed to the optical effect of plamonic Au NPs. In contrast, the electronic characteristic of Au NPs plays a key role in increasing V_{oc} and J_{sc} and thus enhancing the performance of p-PSCs, as discussed below.

Subsequently, to compare the charge carrier dynamics, we performed time-integrated and time-resolved photoluminescence (PL) measurements on perovskite-coated double-layer TiO_2 ETL with and without Au NPs sandwiched within the TiO_2 ETL. It is notable that spiro-OMeTAD is not present in these films. The time-integrated PL spectrum exhibits a significant reduction in the PL for the Au NPs-incorporated sample (**Figure 4b**). The time-resolved PL spectra at the perovskite emission peak of 778 nm are shown in **Figure 4c**. A faster PL quenching was seen the Au NPs-incorporated sample. The bi-exponential fits yield the lifetime τ_1 of 39.46 ns and τ_2 of 135.31 ns for control sample (i.e., no Au NPs sandwiched) and shorter τ_1 of 16.36 ns and τ_2 of 63.42 ns for the Au NPs-incorporated sample. The accelerated PL quenching in the latter suggests a facilitated charge transfer from perovskite to TiO_2.

To further scrutinize the charge carrier dynamics in the device induced by the incorporated Au NPs, we conducted intensity modulated photocurrent spectroscopy (IMPS) and intensity modulated photovoltage spectroscopy (IMVS) measurements as a function of the incident light intensity (**Figure S11**). Both IMPS and IMVS measurements provide insight into the carrier lifetime and charge recombination dynamics, which have been widely used in DSSCs to determine the carrier lifetime (τ_n by IMVS) and charge transit time (τ_d by IMPS). A decreased τ_d and increased τ_n indicate the improved charge transport and carrier collection efficiency.[30-33] **Figure 4d** compares the τ_d and τ_n for the devices with and without sandwiching Au NPs in TiO_2 ETL. Clearly, τ_d of Au NPs-incorporated device is shorter than that of control device at varied incident photon flux, signifying a faster charge transport. The carrier lifetime τ_n reflects the recombination process in p-PSCs. The Au NPs-incorporated device displays a longer τ_n compared to control device. To further uncover the effect of plasmonic NPs on the carrier diffusion, we also calculated the diffusion coefficient of carriers D_n from τ_d and τ_n (**Figure S12**). Obviously, D_n of the Au NPs-incorporated device is increased in comparison to that of control device. Taken together, the introduction of plasmonic Au NPs favors the charge transport, the exciton dissociation, and the carrier mobility (as discussed below), which is consistent with the previous work.[34]

To gain more physical insight into electrical characteristic of p-PSCs, the electrochemical impedance spectroscopy (EIS) was carried out under working condition. **Figure S13a, b** show the Nyquist plots of the devices measured at varied forward biases from 0 to 0.8 V. The high-frequency semicircle is attributed primarily to the contact resistance, and the main semicircle in the low frequency region represents the recombination resistance R_{rec} of charge carriers.[35] An equivalent circuit model (**Figure S13c**) was used to fit the Nyquist plots, from which R_{rec} at various applied biases can be obtained (**Figure S13d**). Clearly, at a fixed bias potential, the R_{rec} of the Au NPs-incorporated device is much larger than that of control device (no Au NPs sandwiched between a double-layer TiO_2), suggesting a markedly improved charge transfer for the Au NPs-incorporated device. This observation accounts for the improved J_{sc} obtained from the *J-V* measurements. The EIS results correlated well with the IMPS and IMVS measurements discussed above. The prolonged lifetime τ_n and reduced transit time τ_d obtained from IMVS and IMPS studies, respectively, are originated from the improved charge transport within the ETL and the facilitated charge transfer and separation at the ETL/perovskite interface.

We note that the promoted charge separation and transport has been reported and ascribed to the reduced exciton binding energy induced by the NEF enhancement of the perovskite film with the incorporation of plasmonic Au/SiO_2 NPs (~8 nm SiO_2 shell) in the mesoporous alumina layer.[20] A reduced exciton binding energy could render charge separation in photoactive perovskite or at the interfaces. However, in the present study with plain Au NPs or Au/SiO_2 NPs with a very thin shell (2 nm SiO_2), the additional possible reason that should be considered is the HET effect. The ability of Au NPs to create plasmonically excited electrons and impart charge transfer has been reported.[19, 36] The accumulated energy induced by the LSPR on plain Au NPs or Au/SiO_2 NPs with an ultrathin shell can effectively dissipate in the form of either re-emitted photons or generated hot electrons.[19, 34] A part of these hot electrons can transfer to the conduction band (CB) of neighboring TiO_2 and even the perovskite absorber, thereby facilitating the carrier transport within the devices.[19, 34, 36, 37] The surface plasmonically excited hot electron flow has been observed in the metal/semiconductor composites.[38] When it comes to the p-PSCs, the most possible dissipation pathway of hot electrons on the Au surface is for them to further interact with TiO_2, thus promoting local electron mobility in the TiO_2 ETL and ultimately leading to improved charge collection.[34, 36] Consequently, the probability of charge transfer at the TiO_2 ETL/perovskite interface and charge transport within the TiO_2 ETL can be largely promoted.

To confirm the increased local electron mobility in TiO_2 ETL induced by the HET effect due to the presence of Au NPs, a structure of FTO/double-layer TiO_2 (presence or absence of Au NPs)/Ag (**Figure S14**) was constructed. A similar device structure for the study of function layers in PSCs has been reported in literature.[39, 40] We simplified the mobility measurement by testing the conductivity difference under the dark and

View Article Online
DOI: 10.1039/C9EE03937F

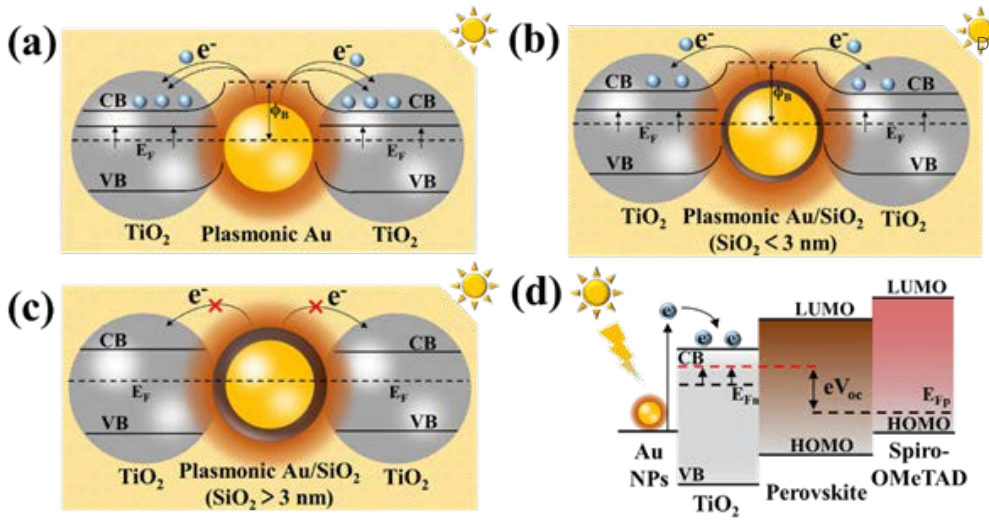

Figure 5. Schematic illustration of LSPR-induced HET and NEF enhancement for plasmonic NPs (Au NP and Au/SiO_2 core/shell NP) sandwiched between a double-layer TiO_2 ETL. (a) TiO_2/Au NP/TiO_2, (b) TiO_2/(Au/SiO_2 NP)/TiO_2 (SiO_2 < 3 nm), and (c) TiO_2/(Au/SiO_2 NP)/TiO_2 (SiO_2 > 3 nm). (d) Schematic diagram of the mechanism of HET process for the trap-filling and the corresponding increased built-in potential of device due to the up-shift of the Fermi level of TiO_2. It is notable that LSPR effect is seen in (a)-(c), and an up-shift in Fermi level as a result of HET process from Au NP to TiO_2 is seen in only (a) and (b). The brown halo in (a)-(c) represents the NEF enhancement. CB and VB are the conduction band and valence band, respectively. ϕ_B in (a)-(b) is the Schottky barrier height between Au and TiO_2. E_F in (a)-(c) is the apparent Fermi level. E_{Fn} and E_{Fp} in (d) are the Fermi level of electrons and holes, respectively. The red dashed line in (d) depicts the elevated Fermi level due to the HET effect.

illumination condition. As illustrated in **Figure 4e**, under the dark condition, the Au NPs-incorporated TiO_2 film shows a slightly increased conductivity compared to the pristine TiO_2 film. In stark contrast, under illumination, the conductivity of both films are enhanced and the Au NPs-incorporated TiO_2 film displays much higher photoconductivity, which favorably impacts the device performance in working condition. We note that the excited hot electrons from Au NPs can transfer to TiO_2 (i.e., HET effect) and fill up the trap states of TiO_2, leading to increased charge carrier density and consequently improved conductivity of TiO_2.[21, 34, 36] On the other hand, the increased carrier density in TiO_2 induced by the HET effect raises the Fermi level of TiO_2 and lowers the work function of TiO_2 (**Figure 4f**), resulting in enhanced built-in potential[19, 37] and thus V_{oc}. To estimate the built-in potential of the devices, the Mott-Schottky analysis was performed at a frequency of 10 kHz with the bias potentials ranging from 0 to 1.2 V.[41, 42] From the x-intercept of the linear regime in the Mott-Schottky plots (**Figure S15**), the built-in potentials of control device and the Au NPs-incorporated device were found to be 0.91 V and 0.94 V, respectively. The increased V_{oc} of the Au NPs-incorporated device is in line with the enhanced built-in potential and the up-shift of Fermi level. Compared to control device with an average V_{oc} of 1.03V, it increases to 1.06 V for the Au NPs-incorporated device (**Table S5**). The devices assembled using Au/SiO_2 NPs with 2 nm SiO_2 shell shows the same trend where the average V_{oc} increases to 1.05 V (**Table S5**). Clearly, the increased V_{oc} is attributed to enhanced built-in potential and decreased energy barrier for carrier transport.

In this context, we propose that the HET from Au NPs to TiO_2 in conjunction with the promoted carrier transfer from perovskite to TiO_2 and charge transport within TiO_2 induced by the NEF enhancement accounts for the improved device performance. The trap states in TiO_2 form an extraction barrier between the photoactive layer and TiO_2, resulting in unfavorable electron extraction. It has been reported that UV-generated electrons in TiO_2 can fill up the trap states and thus enhance the conductivity.[21] The HET process is depicted in **Figure 5a,b**. Upon excitation, hot electrons are generated in Au NPs. The excited hot electrons overcome the Schottky barrier (ϕ_B) between Au NPs and TiO_2 and are injected into the surrounding TiO_2 to passivate the trap states of TiO_2.

In the present study, capping Au core with a SiO_2 shell of different thickness provides a convenient route to assessing the role of plasmonic NPs in PSCs. When Au/SiO_2 NPs with a relatively thicker shell are employed, their influence is limited primarily to the NEF enhancement-induced promotion of carrier transfer from perovskite to TiO_2 and charge transport within TiO_2 (**Figure 5c**). It is important to note that such effect does not alter the apparent Fermi level of the double-layer TiO_2 film. If plain Au or Au/SiO_2 NPs of a very thin SiO_2 shell are in contact with TiO_2, they are capable of transferring hot electrons to the neighboring TiO_2 and undergoing the Fermi level equilibration.[19, 37] The Fermi level up-shift results in a longer electron lifetime and a higher recombination resistance, ultimately leading to improved charge transport and increased V_{oc} (**Figure 5d**). Notably, earlier reports on plasmonic PSCs have demonstrated a clear increase in V_{oc} of approximately 10-30 mV by exploiting Ag/TiO_2[43] and Au NPs[44].

Effectiveness of the TiO_2/Au NPs/TiO_2 ETL in mesostructured PSCs.

In addition to the planar PSCs discussed above, to demonstrate the effectiveness of the TiO_2/Au NPs/TiO_2 ETL in tailoring charge carrier dynamics of PSCs, we also capitalized on the sandwich-like ETL for mesostructured PSCs (denoted m-PSCs) by adding

View Article Online
DOI: 10.1039/C9EE03775

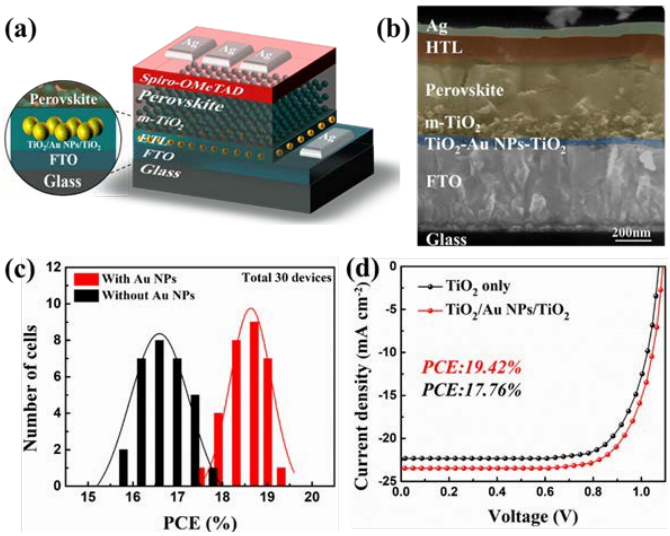

Figure 6. (a) Device configuration and (b) cross sectional SEM image of mesostructured PSC (denoted m-PSC) assembled using $FA_{0.85}MA_{0.15}PbI_{2.55}Br_{0.45}$ as absorber and TiO_2/Au NPs/TiO_2 as ETL. (c) The statistics of PCEs for 30 m-PSCs assembled using $FA_{0.85}MA_{0.15}PbI_{2.55}Br_{0.45}$ as absorber with and without Au NPs sandwiched between a double-layer TiO_2 as ETL, respectively. (d) *J-V* characteristics of the champion m-PSCs assembled using $FA_{0.85}MA_{0.15}PbI_{2.55}Br_{0.45}$ as absorber with (PCE = 19.42%) and without (PCE = 17.76%) Au NPs sandwiched between a double-layer TiO_2 as ETL, respectively.

an additional mesoporous TiO_2 layer on the sandwiched TiO_2/Au NPs/TiO_2 film (**Figure 6a,b**). **Figure 6c** and **Figure S16** present the statistics of photovoltaic characteristics of m-PSCs based on $FA_{0.85}MA_{0.15}PbI_{2.55}Br_{0.45}$ absorber assembled with the TiO_2/Au NPs/TiO_2 and TiO_2/TiO_2 (i.e., control sample) ETLs. The most probable J_{sc} of 22.3 mA cm^{-2} and V_{oc} of 1.07 V are achieved from the device based on TiO_2/Au NPs/TiO_2 ETL, which are much higher than those of control device (J_{sc} = 20.9 mA cm^{-2} and V_{oc} = 1.04 V) (**Figure S16a,b**). It is worth noting that the optimal m-PSC constructed by using $FA_{0.85}MA_{0.15}PbI_{2.55}Br_{0.45}$ as absorber and TiO_2/Au NPs/TiO_2 as ETL deliver a markedly enhanced PCE of 19.42%, compared to that of optimal control device (PCE = 17.76%) (**Figure 6d**).

Device stability.

Due to effective charge trap passivation of TiO_2 via HET from Au NPs, the issues associated with interfacial reaction and the ion migration in PSCs can be alleviated, thereby improving the device stability.[45] Both p-PSCs and m-PSCs with and without Au NPs sandwiched between a double-layer TiO_2 were stored in the desiccator without encapsulation and evaluated under ambient condition (temperature: 25 ± 2 °C, relative humidity: 30 ± 5%) (**Figure S17**). For control devices (no Au NPs incorporated), they only retain 68.8% and 57.6% of their original PCEs after one-month for p-PSCs and m-PSCs, respectively. In stark contrast, the devices with introduced Au NPs manifest an improved durability, experiencing only 14.5% and 17.8% PCE loss for p-PSCs and m-PSCs, respectively.

Conclusions

In summary, we developed an understanding on how judicious design of plasmonic NPs of different dimension and architecture as well as their interfacial positioning facilitates the tailoring of charge carrier dynamics in PSCs. Such investigation is enabled by the use of amphiphilic star-like block copolymer nanoreactors to craft monodisperse plain Au and Au/SiO_2 core/shell NPs with a fixed Au core diameter and varied SiO_2 shell thickness. The presence of SiO_2 shell exerts a profound influence on J_{sc} and V_{oc} of PSCs. When sandwiching Au/SiO_2 core/shell NPs within TiO_2 ETL, the resulting PSCs containing Au/SiO_2 core/shell NPs with 6 nm and 10 nm thick SiO_2 shell produces only higher J_{sc} compared to control device constructed in the absence of Au or Au/SiO_2 NPs sandwiched between a double-layer TiO_2 ETL. In stark contrast, both plain Au NPs and Au/SiO_2 NPs with a very thin SiO_2 shell of 2 nm experience the HET that passivates the trap states in TiO_2, leading to improved charge transfer from perovskite to TiO_2 and transport within the TiO_2 ETL and thus increased J_{sc}. Moreover, the HET process also leads to increased carrier density in TiO_2 that shift the Fermi level of TiO_2 upward, resulting in increased V_{oc}. Taken together, both J_{sc} and V_{oc} for plain Au NPs and Au/SiO_2 NPs with the SiO_2 shell thickness t_{SiO2} of 2 nm are much larger than those of the abovementioned cases (i.e., t_{SiO2} of 6 nm and 10 nm). Consequently, the optimal planar and mesostructured PSCs engineered using the TiO_2/Au NPs/TiO_2 ETL (i.e., plain Au NPs sandwiched between a double-layer TiO_2) yield the champion PCEs of 18.81% and 19.42%, respectively (scenario 1). Notably, the devices fabricated by impregnating Au NPs via scenario 1 outperform those by placing plasmonic NPs at the perovskite/TiO_2 interface (scenario 2). This study offers insight into the tailoring of charge carrier dynamics in PSCs via rational design and placement of monodisperse plasmonic/dielectric NPs with tunable dielectric shell thickness to achieve plasmonic enhancement-enabled high-performance PSCs. Moreover, as precursors amenable to the star-like block copolymer nanoreactor strategy is virtually unlimited, conceptually a myriad of functional NPs with accurately controlled sizes, architectures, and composition can be readily created for use in solar-to-chemical energy conversion, controlled nanoscale light-matter interaction, etc.

Conflicts of interest

There are no conflicts to declare.

Acknowledgements

This work is supported by the Air Force Office of Scientific Research (FA9550-19-1-0317), and the National Science Foundation (ECCS 1914562). Both Y. Y. and X. C. acknowledge the financial support from the National Natural Science Foundation of China (51973235, 51673061, and 51273057).

Notes and references

DOI: 10.1039/C9EE03937F

1. NREL's "Best Research-Cell Efficiencies" Chart, https://www.nrel.gov/pv/cell-efficiency.html.
2. M. He, D. Zheng, M. Wang, C. Lin and Z. Lin, *J. Mater. Chem. A*, 2014, **2**, 5994-6003.
3. X. Liu, Y. Wang, X. Cui, M. Zhang, B. Wang, M. Rager, Z. Shu, Y. Yang, Z. Li and Z. Lin, *J. Mater. Chem. A*, 2019, **7**, 165-171.
4. A. Kojima, K. Teshima, Y. Shirai and T. Miyasaka, *J. Am. Chem. Soc.*, 2009, **131**, 6050-6051.
5. W. Chen, Y. Wu, Y. Yue, J. Liu, W. Zhang, X. Yang, H. Chen, E. Bi, I. Ashraful and M. Grätzel, *Science*, 2015, **350**, 944-948.
6. W. S. Yang, B.-W. Park, E. H. Jung, N. J. Jeon, Y. C. Kim, D. U. Lee, S. S. Shin, J. Seo, E. K. Kim and J. H. Noh, *Science*, 2017, **356**, 1376-1379.
7. B. Wang, J. Iocozzia, M. Zhang, M. Ye, S. Yan, H. Jin, S. Wang, Z. Zou and Z. Lin, *Chem. Soc. Rev.*, 2019, **48**, 4854-4891.
8. M. He, B. Li, X. Cui, B. Jiang, Y. He, Y. Chen, D. O'Neil, P. Szymanski, M. A. Ei-Sayed, J. Huang and Z. Lin, *Nat. Commun.*, 2017, **8**, 16045.
9. M. Yang, T. Zhang, P. Schulz, Z. Li, G. Li, D. H. Kim, N. Guo, J. J. Berry, K. Zhu and Y. Zhao, *Nat. Commun.*, 2016, **7**, 12305.
10. D. P. McMeekin, G. Sadoughi, W. Rehman, G. E. Eperon, M. Saliba, M. T. Hörantner, A. Haghighirad, N. Sakai, L. Korte and B. Rech, *Science*, 2016, **351**, 151-155.
11. Q. Chen, H. Zhou, T.-B. Song, S. Luo, Z. Hong, H.-S. Duan, L. Dou, Y. Liu and Y. Yang, *Nano Lett.*, 2014, **14**, 4158-4163.
12. M. Ye, C. He, J. Iocozzia, X. Liu, X. Cui, X. Meng, M. Rager, X. Hong, X. Liu and Z. Lin, *J. Phys. D: Appl. Phys.*, 2017, **50**, 373002.
13. H. Zhou, Q. Chen, G. Li, S. Luo, T.-b. Song, H.-S. Duan, Z. Hong, J. You, Y. Liu and Y. Yang, *Science*, 2014, **345**, 542-546.
14. M. D. Brown, T. Suteewong, R. S. S. Kumar, V. D'Innocenzo, A. Petrozza, M. M. Lee, U. Wiesner and H. J. Snaith, *Nano Lett.*, 2010, **11**, 438-445.
15. J. Qi, X. Dang, P. T. Hammond and A. M. Belcher, *ACS nano*, 2011, **5**, 7108-7116.
16. X. Liu, J. Iocozzia, Y. Wang, X. Cui, Y. Chen, S. Zhao, Z. Li and Z. Lin, *Energy Environ. Sci.*, 2017, **10**, 402-434.
17. K. Awazu, M. Fujimaki, C. Rockstuhl, J. Tominaga, H. Murakami, Y. Ohki, N. Yoshida and T. Watanabe, *J. Am. Chem. Soc.*, 2008, **130**, 1676-1680.
18. N. Aeineh, E. M. Barea, A. Behjat, N. Sharifi and I. Mora-Sero, *ACS Appl. Mater. Interfaces*, 2017, **9**, 13181-13187.
19. Z. Yuan, Z. Wu, S. Bai, Z. Xia, W. Xu, T. Song, H. Wu, L. Xu, J. Si and Y. Jin, *Adv. Energy Mater.*, 2015, **5**, 1500038.
20. W. Zhang, M. Saliba, S. D. Stranks, Y. Sun, X. Shi, U. Wiesner and H. J. Snaith, *Nano Lett.*, 2013, **13**, 4505-4510.
21. C. S. Kim, S. S. Lee, E. D. Gomez, J. B. Kim and Y.-L. Loo, *Appl. Phys. Lett.*, 2009, **94**, 84.
22. A. O. Govorov, H. Zhang and Y. K. Gun'ko, *J. Phys. Chem. C*, 2013, **117**, 16616-16631.
23. W. R. Erwin, A. Coppola, H. F. Zarick, P. Arora, K. J. Miller and R. Bardhan, *Nanoscale*, 2014, **6**, 12626-12634.
24. Y. J. Yoon, Y. Chang, S. Zhang, M. Zhang, S. Pan, Y. He, C. H. Lin, S. Yu, Y. Chen, Z. Wang, Y. Ding, J. Jung, N. Thadhani, V. V. Tsukruk, Z. Kang and Z. Lin, *Adv. Mater.*, 2019, **31**, e1901602.
25. X. Li, J. Iocozzia, Y. Chen, S. Zhao, X. Cui, W. Wang, H. Yu, S. Lin and Z. Lin, *Angew. Chem. Int. Ed.*, 2018, **57**, 2046-2070.
26. X. Pang, L. Zhao, W. Han, X. Xin and Z. Lin, *Nat. Nanotechnol.*, 2013, **8**, 426-431.
27. K. Matyjaszewski and N. V. Tsarevsky, *Nat. Chem.*, 2009, **1**, 276-288.
28. K. Chan, M. Wright, N. Elumalai, A. Uddin and S. Pillai, *Adv. Opt. Mater.*, 2017, **5**, 1600698.
29. A. Guerrero, S. Chambon, L. Hirsch and G. Garcia‐Belmonte, *Adv. Funct. Mater.*, 2014, **24**, 6234-6240.
30. J. H. Heo, D. H. Song, H. J. Han, S. Y. Kim, J. H. Kim, D. Kim, H. W. Shin, T. K. Ahn, C. Wolf and T. W. Lee, *Adv. Mater.*, 2015, **27**, 3424-3430.
31. J. H. Heo, H. J. Han, D. Kim, T. K. Ahn and S. H. Im, *Energy Environ Sci*, 2015, **8**, 1602-1608.
32. M. Cha, P. Da, J. Wang, W. Wang, Z. Chen, F. Xiu, G. Zheng and Z.-S. Wang, *J. Am. Chem. Soc.*, 2016, **138**, 8581-8587.
33. X. Meng, X. Cui, M. Rager, S. Zhang, Z. Wang, J. Yu, Y. W. Harn, Z. Kang, B. K. Wagner, Y. Liu, C. Yu, J. Qiu and Z. Lin, *Nano Energy*, 2018, **52**, 123-133.
34. R. Fan, L. Wang, Y. Chen, G. Zheng, L. Li, Z. Li and H. Zhou, *J. Mater. Chem. A*, 2017, **5**, 12034-12042.
35. M. He, X. Pang, X. Liu, B. Jiang, Y. He, H. Snaith and Z. Lin, *Angew. Chem. Int. Ed.*, 2016, **55**, 4280-4284.
36. W. R. Erwin, H. F. Zarick, E. M. Talbert and R. Bardhan, *Energy Environ. Sci.*, 2016, **9**, 1577-1601.
37. D. Zhang, W. C. Choy, F. Xie, W. E. Sha, X. Li, B. Ding, K. Zhang, F. Huang and Y. Cao, *Adv. Funct. Mater.*, 2013, **23**, 4255-4261.
38. Y. K. Lee, C. H. Jung, J. Park, H. Seo, G. A. Somorjai and J. Y. Park, *Nano Lett.*, 2011, **11**, 4251-4255.
39. R. O'Hayre, M. Nanu, J. Schoonman and A. Goossens, *J. Phys. Chem. C*, 2007, **111**, 4809-4814.
40. S. van Reenen, M. Kemerink and H. J. Snaith, *J. Phys. Chem. Lett.*, 2015, **6**, 3808-3814.
41. A. Guerrero, E. J. Juarez-Perez, J. Bisquert, I. Mora-Sero and G. Garcia-Belmonte, *Appl. Phys. Lett.*, 2014, **105**, 133902.
42. T. Bu, J. Li, F. Zheng, W. Chen, X. Wen, Z. Ku, Y. Peng, J. Zhong, Y. B. Cheng and F. Huang, *Nat. Commun.*, 2018, **9**, 4609.
43. M. Saliba, W. Zhang, V. M. Burlakov, S. D. Stranks, Y. Sun, J. M. Ball, M. B. Johnston, A. Goriely, U. Wiesner and H. J. Snaith, *Adv. Funct. Mater.*, 2015, **25**, 5038-5046.
44. S. S. Mali, C. S. Shim, H. Kim, P. S. Patil and C. K. Hong, *Nanoscale*, 2016, **8**, 2664-2677.
45. H. Dong, T. Lei, F. Yuan, J. Xu, Y. Niu, B. Jiao, Z. Zhang, D. Ding, X. Hou and Z. Wu, *Org. Electron.*, 2018, **60**, 1-8.

Table of contents

View Article Online
DOI: 10.1039/C9EE03937F

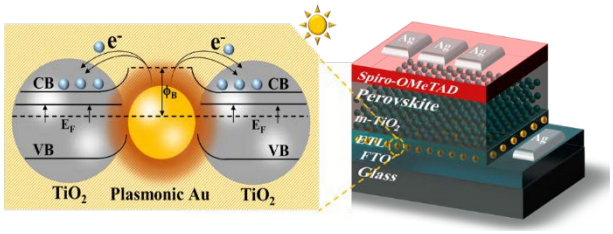

The judicious positioning of rationally designed monodisperse plasmonic NPs in ETL affords effective tailoring of carrier dynamics of PSCs.